REPORT DOCUMENTATION PAGE

Form Approved
OMB No. 0704-0188

1. REPORT DATE *(DD-MM-YYYY)*	2. REPORT TYPE	3. DATES COVERED *(From - To)*
02/29/2008	Final	01 Jun 03 to 30 November 07

4. TITLE AND SUBTITLE
High-efficiency helical coil electromagnetic launcher and high power Hall-effect switch

5a. CONTRACT NUMBER ~~F49620-03-1-0350~~ FA9550-06-1-0448

5b. GRANT NUMBER

5c. PROGRAM ELEMENT NUMBER

6. AUTHOR(S)
Thomas G. Engel, William C. Nunnally, John M. Gahl

5d. PROJECT NUMBER

5e. TASK NUMBER

5f. WORK UNIT NUMBER

7. PERFORMING ORGANIZATION NAME(S) AND ADDRESS(ES)

Univ. Missouri-Columbia
College of Engineering
Dept of Electrical Engineering

8. PERFORMING ORGANIZATION REPORT NUMBER

9. SPONSORING / MONITORING AGENCY NAME(S) AND ADDRESS(ES)
AFOSR/NE
4015 Wilson Blvd.
Room 713
Arlington, VA 22203-1954

10. SPONSOR/MONITOR'S ACRONYM(S)

11. SPONSOR/MONITOR'S REPORT

AFRL-SR-AR-TR-08-0141

12. DISTRIBUTION / AVAILABILITY STATEMENT
Distribution Statement A: Unlimited

13. SUPPLEMENTARY NOTES
Final report during the reporting period includes the development of new theory of operation for electromagnetic launcher applicable to all constant inductance gradient launcher geometries. Theory develops expressions for efficiency and methods to predict the performance of different geometry electromagnetic launchers allowing them to be compared to each other. A theoretical analysis is also presented to design a helical electromagnetic launcher for a specific volt-amp characteristic. Experimentally measured performance is reported for a 40 millimeter bore helical electromagnetic launcher which is subsequently compared to a one-turn augmented railgun and a conventional railgun operating at comparable scale. Experimental results are also given that demonstrate significant launcher performance benefits by super-cooling the armature (i.e., using liquid nitrogen).

14. ABSTRACT

Efficiency and scaling relationships for DC (i.e., non-induction) constant inductance gradient electromagnetic launchers are presented and discussed. Expressions for electromagnetic force, efficiency, back-voltage, and kinetic power are derived and given in terms of electrical circuit parameters. Launcher efficiency is shown to be a simple function of armature velocity and the launcher's characteristic velocity. The characteristic velocity characterizes the launcher and is the product of two new parameters; the mode constant and launcher constant. Mathematically, the launcher must operate at its characteristic velocity for 50% maximum efficiency. The mode constant reflects the manner in which the launcher is powered and its maximum efficiency. The launcher constant reflects the geometry of the launcher. The two modes of operation presented in this investigation include constant current and zero exit current operation. The ideal electromagnetic launcher concept is developed and defined by operation at 100% maximum efficiency at all velocities. The concept of same-scale comparisons is developed and states that electromagnetic launcher comparisons should be done with equal bore diameter, launcher length, projectile mass, and velocity. A comparative analysis using experimental data of same-scale constant gradient electromagnetic launchers is performed with conventional railgun, augmented railgun, and helical gun launchers and is presented in terms of the launcher constant, inductance gradient, bore diameter, bore length, system resistance, and armature (i.e., projectile) velocity. A theoretical analysis is also presented to design a helical electromagnetic launcher for a specific volt-amp characteristic. Experimentally measured performance is reported for a 40 millimeter bore helical electromagnetic launcher which is subsequently compared to a one-turn augmented railgun and a conventional railgun operating at comparable scale. Experimental results are also given that demonstrate significant launcher performance benefits by super-cooling the conductor in the armature (i.e., liquid nitrogen temperatures). A computer model for a magnetically-controlled Hall-effect switch is developed. The model is constructed in the PSpice circuit simulation software. Results from the switch model are compared to experimentally measured parameters. There is good agreement between theory and experiment. The switch model is useful to determine usefulness of Hall-effect devices in electromagnetic launcher applications.

15. SUBJECT TERMS

16. SECURITY CLASSIFICATION OF:			**17. LIMITATION OF ABSTRACT**	**18. NUMBER OF PAGES**	**19a. NAME OF RESPONSIBLE PERSON**
					Thomas G. Engel
a. REPORT	**b. ABSTRACT**	**c. THIS PAGE**			**19b. TELEPHONE NUMBER** *(include area code)* (573) 882-2972

Standard Form 298 (Rev. 8-98)
Prescribed by ANSI Std. Z39.18

Final Report: High-Efficiency Helical Coil Electromagnetic Launcher and High Power Hall-Effect Switch

by
T.G. Engel, W.C. Nunnally, and J.M. Gahl
Center for Energy Conversion and Electromagnetics
Department of Electrical and Computer Engineering
University of Missouri
Columbia, MO 65211

Contract: ~~F49620-03-1-0350~~
FA9550-06-1-0448

29 February 2008

Table of Contents

Executive Summary

The research effort has produced a new high energy (750 kJ) electromagnetic launcher (EML) facility at the University of Missouri-Columbia (MU). This new facility will be used in the future to test prototype EML's of all geometry types including rail, augmented rail, and helical. The research has also produced new modeling techniques for magnetically-controlled Hall-effect switches and devices. Hall-effect devices could be useful in electromagnetic launcher applications due to the large magnetic fields present.

The research effort has produced a new theoretical understanding of efficiency and scaling for al types of constant gradient EML's. EML efficiency is shown to be a simple function of armature velocity and the launcher's characteristic velocity. The concept of an ideal EML is developed and defined by operation at 100% maximum efficiency at all velocities. The concept of same-scale comparisons is developed and states that EML comparisons should be done with equal bore diameter, launcher length, projectile mass, and velocity. A comparative analysis using experimental data of same-scale constant gradient EML's is performed with conventional railgun, augmented railgun, and helical gun launchers and is presented in terms of the launcher constant, inductance gradient, bore diameter, bore length, system resistance, and armature (i.e., projectile) velocity. General EML design guidelines are developed which emphasize the election of the EML V-I operating point. The beneficial effect of super-cooling is demonstrated with liquid nitrogen cooling and indicates super-cooled EML operation is desirable if cryo-cooling is practical for the application.

The research effort has also produced new modeling techniques for magnetically-controlled Hall-effect switches and devices. Hall-effect devices could be useful in electromagnetic launcher applications due to the large magnetic fields present. The Hall-effect switch model is developed in the PSpice circuit simulation code giving the engineer the ability to study device physics as well as the device behavior in circuits and systems. An analysis was performed comparing model results with the experimentally measured magnetoresistance. There was good agreement between predicted and measured results.

Graduate students fully or partly supported by the research include C. Keawboonchuay (PhD), S. Huenefeldt (MS), S. Rohe (MS), C. Nunnally (PhD). Faculty include T.G. Engel, W.C. Nunnally, J.M. Gahl. A list of journal, conference, thesis, and dissertation publications is given below:

Journal publications (students underlined):

1. W. Clay Nunnally, S. M. Huenefeldt, and T.G. Engel, "Performance and scalability of MJ sequentially-fired pulse forming networks for linear and non-linear loads," IEEE Transactions on Plasma Science, vol. 35, no. 2, pp. 484-490, 2007.

2. T.G. Engel, J. M. Neri, W.C. Nunnally, "Efficiency and scaling of constant inductance gradient DC electromagnetic launchers," IEEE Transactions on Magnetics, vol. 42, no. 8, pp 2043 – 2051, 2006.
3. T.G. Engel and S. Rohe , "A comparison of single-layer coaxial coil mutual inductance calculations using finite element and tabulated methods," IEEE Transactions on Magnetics, vol. 42, no. 9, pp. 2159 – 2163, 2006.
4. T.G. Engel and W. Clay Nunnally, "Design and operation of a sequentially-fired pulse forming network for non-linear loads," IEEE Transactions on Plasma Science, vol. 33, no. 6, pp 2060 – 2065, 2005.
5. T.G. Engel, W.C. Nunnally, and J. Neri, "Development of a medium-bore high-efficiency helical coil electromagnetic launcher," IEEE Transactions on Magnetics, vol. 41, no. 11, pp 4299 – 4303, 2005.
6. T.G. Engel, W.C. Nunnally, and J.M. Neri, "Development of a medium bore high efficiency helical coil electromagnetic launcher," IEEE Transactions on Plasma Science, vol. 32, no. 5, pp. 1893 - 1895, 2004.

Conference publications and presentations (students underlined):

1. T.G. Engel, J.M. Neri, M.J. Veracka, "Solid-projectile helical coil electromagnetic launchers," Proc. 16th IEEE International Pulsed Power Conference, pp. 1789-1792, 2007.
2. T.G. Engel, J.M. Neri, M.J. Veracka, "Increased lifetime through current reduction in high efficiency helical coil electromagnetic launchers," Institute for Advanced Technology Classified Seminar on the Applications of Electromagnetic Launch Technology, May 2007, Washington, DC.
3. T.G. Engel, J.M. Neri, and W.C. Nunnally, "A same-scale comparison of electromagnetic launchers," *Invited Paper*, Proc. of the 27th IEEE International Power Modulator Conference, May, 2006.
4. C.S. Pinkston and T.G. Engel, "Maximum charge generation in a piezoelectric generator," Proc. of the 27th IEEE International Power Modulator Conference, May, 2006.
5. W. Clay Nunnally, S. M. Huenefeldt, and T.G. Engel, "Results from a 750 kJ computer controlled sequentially-fired pulse forming network," Proc. of the 27th IEEE International Power Modulator Conference, May, 2006.
6. T.G. Engel, W.C. Nunnally, J.M. Gahl, and W. Clay Nunnally, "Efficiency and scaling in DC electromagnetic launchers," Proc. of the 15th IEEE International Pulsed Power Conference, June 2005.
7. T.G. Engel, W.C. Nunnally, J.M. Gahl, and W. Clay Nunnally, "Medium-bore helical-coil electromagnetic launcher with a liquid nitrogen cooled armature," Proc. of the 15th IEEE International Pulsed Power Conference, June 2005.
8. S. M. Huenefeldt, T. G. Engel, and W. Clay Nunnally, A 750 kJ computer controlled sequentially-fired pulse forming network for a helical coil electromagnetic launcher," Proc. of the 15th IEEE International Pulsed Power Conference, June 2005.

Thesis and dissertation publications:

1. S. Heunefeldt, "A 750 kJ sequentially fired pulse forming network for helical coil electromagnetic launcher," MS Thesis, University of Missouri-Columbia, December, 2006.
2. S. Rohe, "Investigation of the accuracy of Grover's method when solving for the mutual inductance of two single-layer coaxial coils," MS Thesis, University of Missouri-Columbia, December 2005.
3. C. Nunnally, "Investigation of magneto-resistive devices (tentative)," PhD Dissertation, University of Missouri-Columbia, (in progress), May, 2008.

Experimental Arrangement and Procedure

The section below describes the experimental arrangement and procedure used in the research. Two experimental pulse forming networks (PFN's) are used with 125 kJ and 750 kJ total stired energy, respectively. Both PFN's are modularized in construction to accommodate a wide variety of load V-I characteristics.

A set of two high-speed framing camera is common to both experimental arrangements. The first high-speed framing camera is an Imacon 200 from DRS Hadlund. This camera is able to capture a total of 12 frames at up to 200,000,000 frames per second speeds and. Expsoure times are variable down to a minimum of 5ns exposure time. The frames are digital images with 1280 x 1024 resolution. The camera is an excellent addition to the diagnostic capability of the laboratory. The second high-speed framing camera is the Phantom v.7.1 from Vision Research. It uses a 12-bit 800 x 600 color CCD which can record 4,800 uninterpolated frames per second at that resolution. The Phantom can record a maximum of 150,000 fps at a lower spatial resolution. The on-board memeory allows the camera to record up to 4 seconds of a particular event. The set of high-speed cameras have been successfully used to diagnose several HCEL operational problems that would have not been possible otherwise. For example, the armature coil housing was mechanically stretched by the high-force launch causing a de-coupling of forces. We were able to see verify this event with the high-speed camera.

125 kJ Modularized Pulsed Power Supply and Data Acquisition System

The 125 kJ modularized pulsed power supply consists of 8 identical pulse-forming networks (PFN's) that are independently charged to various voltage levels and sequentially fired into the helical coil electromagnetic launcher (i.e., HCEL). The HCEL is a highly non-linear load due to resistance increases caused by joule heating in the windings and due to terminal voltage increases caused by increases in the back-voltage. The variable voltage level charging allows the current to be held at a constant level despite these non-linear load changes. The modularized pulsed power supply has 125 kJ total stored energy capability. We have successfully demonstrated the delivery of relatively constant 15 kA pulses over 8 ms period. The concept can be used in other applications where non-linear pulsed power loads are used. Table I lists the operating characteristics of the 125 kJ sequentially-fired pulse forming network (SFPFN).

Fig 1 shows the 125 kJ SFPFN and its constituent parts connected to a 40 mm bore HCEL. Fig 2 shows the computerized data acquisition system used in this facility.

TABLE I
125 kJ SFPFN OPERATING CHARACTERISTICS

Parameter	Value
Voltage (max)	900 V
Current (max)	50 kA
Equivalent capacitance	0.308 F
Equivalent series inductance	1 μH
Equivalent series resistance	~ 1 mΩ

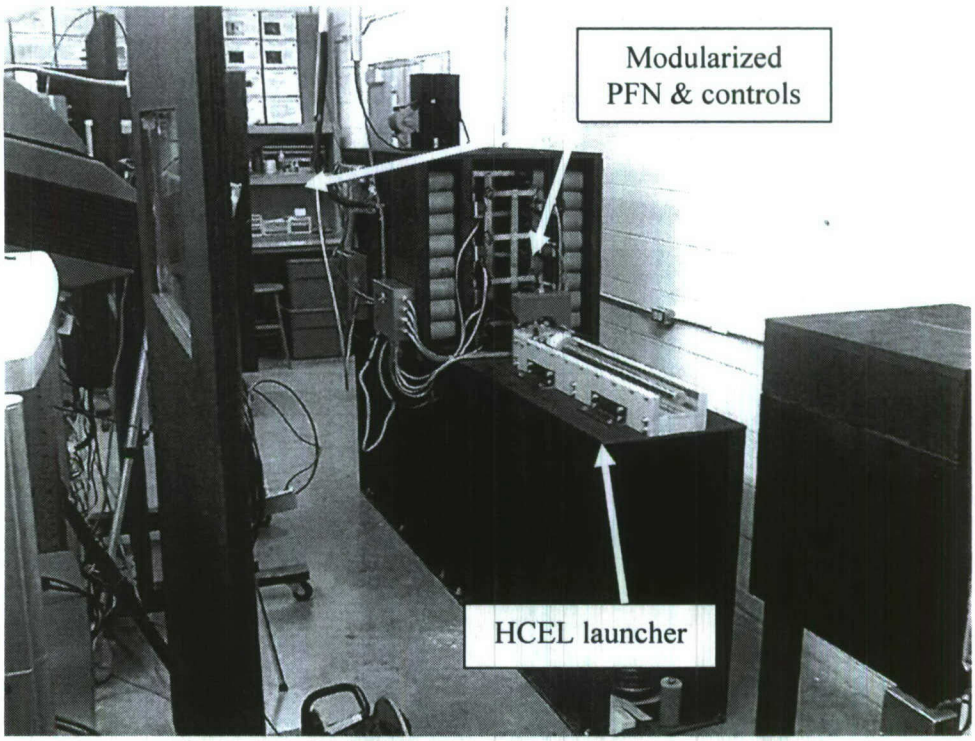

Fig 1. 125 kJ SFPFN connected to a 40 mm HCEL.

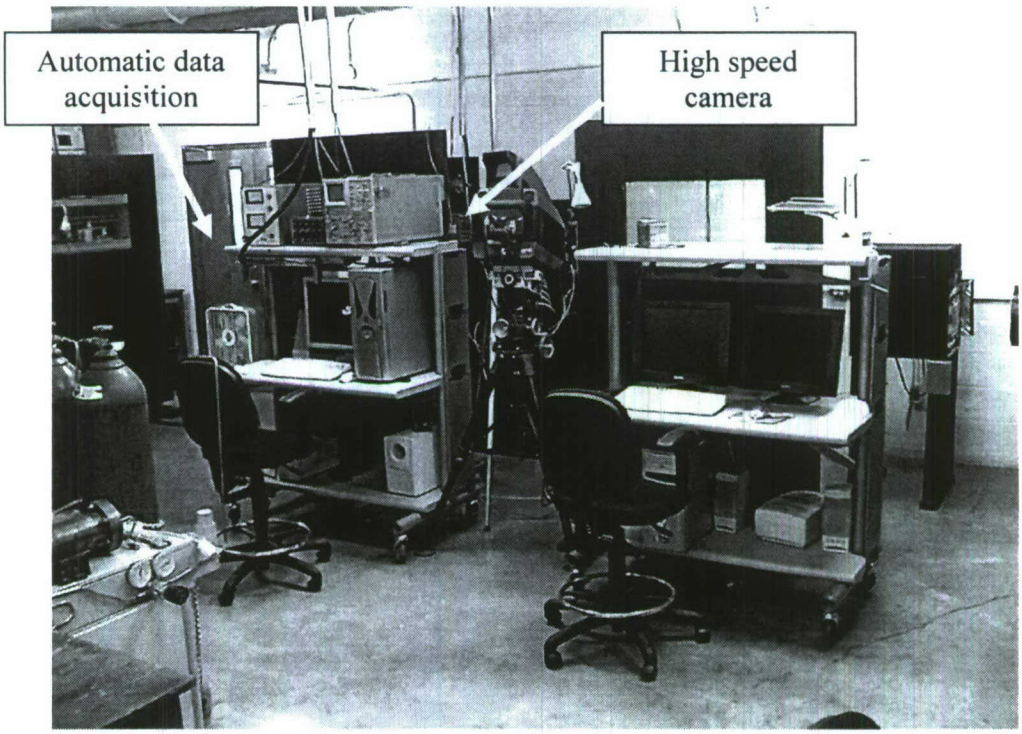

Fig 2. Computerized data acquisition system and high-speed camera.

750 kJ Modularized Pulsed Power Supply and Data Acquisition System

A new 750 kJ SFPFN was constructed during the course of this experiment consisting of 6 non-identical pulse-forming networks (PFN's) that are independently charged to various voltage levels and sequentially fired into the HCEL. The modularized pulsed power supply has 750 kJ total stored energy capability. We have successfully test fired the system verifying its operation and data acquisition systems but have used it with an EML load. Table II lists the operating characteristics of the 125 kJ sequentially-fired pulse forming network (SFPFN).

TABLE II
750 kJ SFPFN OPERATING CHARACTERISTICS

Parameter	Value
Voltage (max)	3000 V
Current (max)	500 kA
Equivalent capacitance	N.A.
Equivalent series inductance	1 μH
Equivalent series resistance	~ 3 mΩ

Fig 3 shows the 750 kJ SFPFN and its constituent parts. Fig 4 shows the various other components associated with this facility.

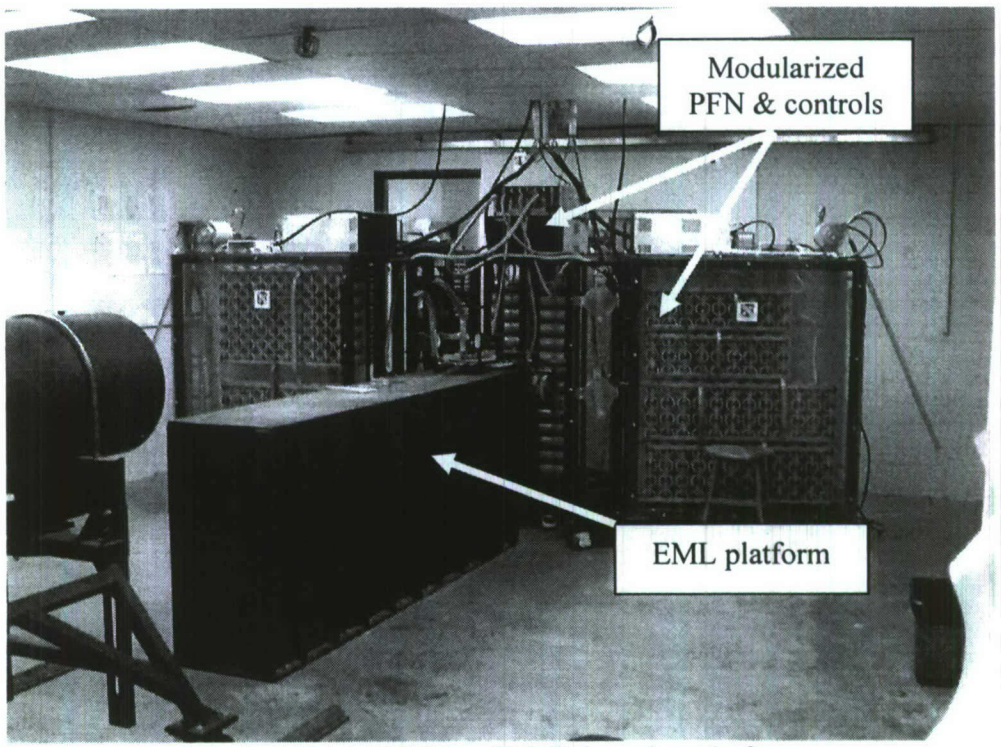

Fig 3. 750 kJ SFPFN and EML launcher platform.

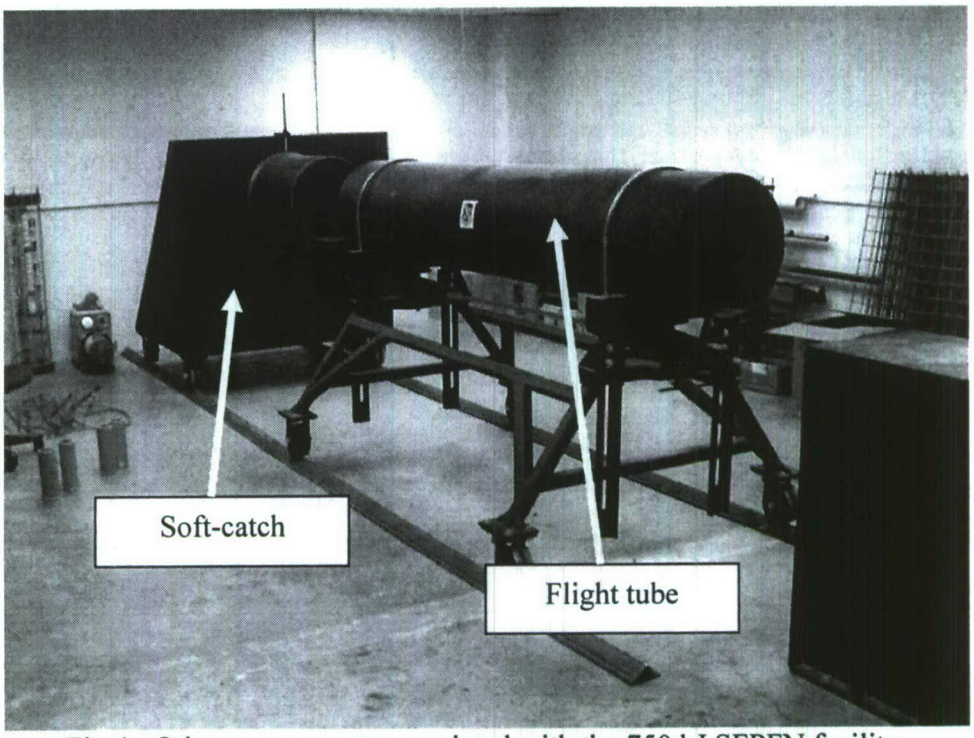

Fig 4. Other components associated with the 750 kJ SFPFN facility.

Helical Electromagnetic Launcher

Fig 5 shows the 40 mm bore HCEL used in the research while Fig 6 shows a close-up view of the projectile. Sponsorship for construction of the HCEL was funded by another contract [1]. Table III lists the physical dimensions of the HCEL. Later sections of this report give more details of the HCEL and projectile.

TABLE III
CONSTRUCTION PARAMETERS OF THE 40 mm HCEL

Parameter	Value
Length	0.75 m
Diameter	40 mm
Projectile mass	350 to 500 g
Projectile length	89 mm
Projectile O.D.	75 mm

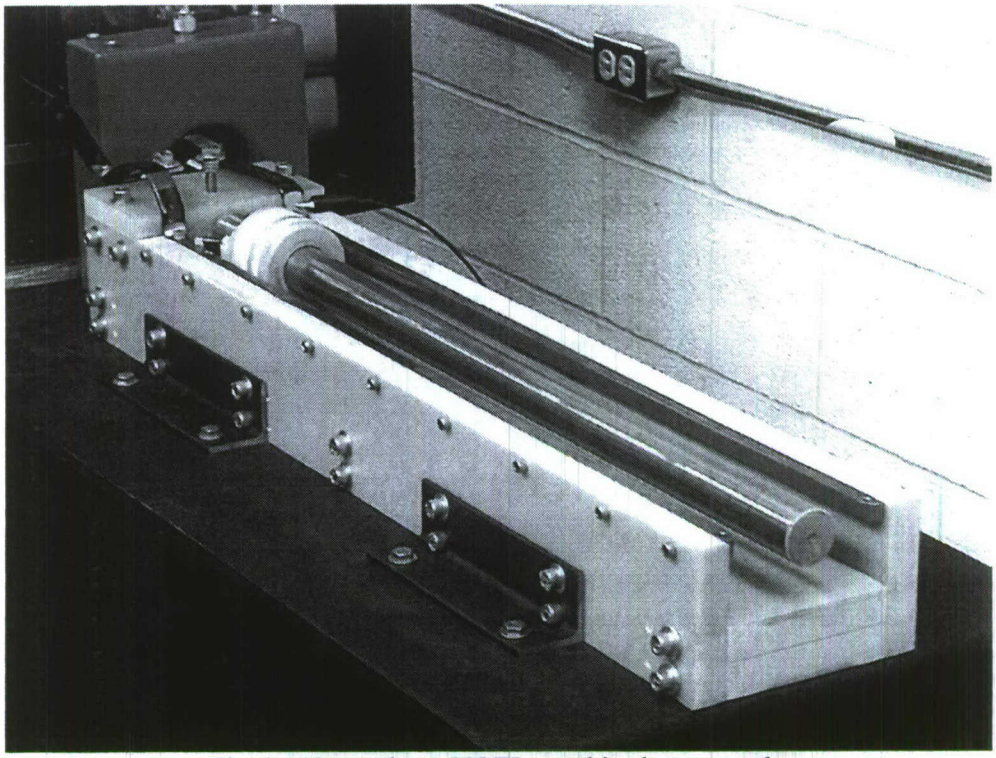

Fig 5. 40 mm bore HCEL used in the research.

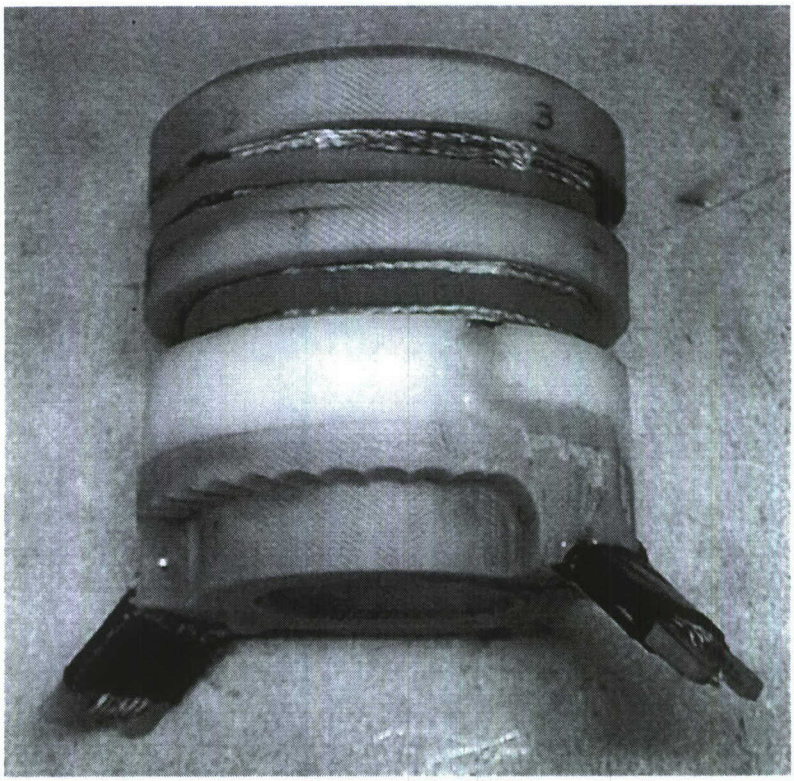

Fig 6. Close-up view of the HCEL projectile.

Experimental Results

The experimental results of the research are given in the sections below. Experimental data are included to support the theoretical development in this section where appropriate..

General Theory of Electromagnetic Launcher Efficiency

The following electromagnetic launcher efficiency analysis uses the three constant gradient electromagnetic launcher (EML) geometries of the conventional railgun, augmented railgun, and helical gun shown in Fig 7.

Electromagnetic Force

Electromagnetic force generated by any electromechanical system is defined as the gradient of the inductively stored energy [1] and expressed mathematically as

$$F \triangleq \nabla W_i \tag{1}$$

where F is the electromagnetic force and W_i is the inductively stored electrical energy stored internally in the launcher. Applying (1) to the conventional and augmented railguns of Fig 7(a) and 1(b) yields

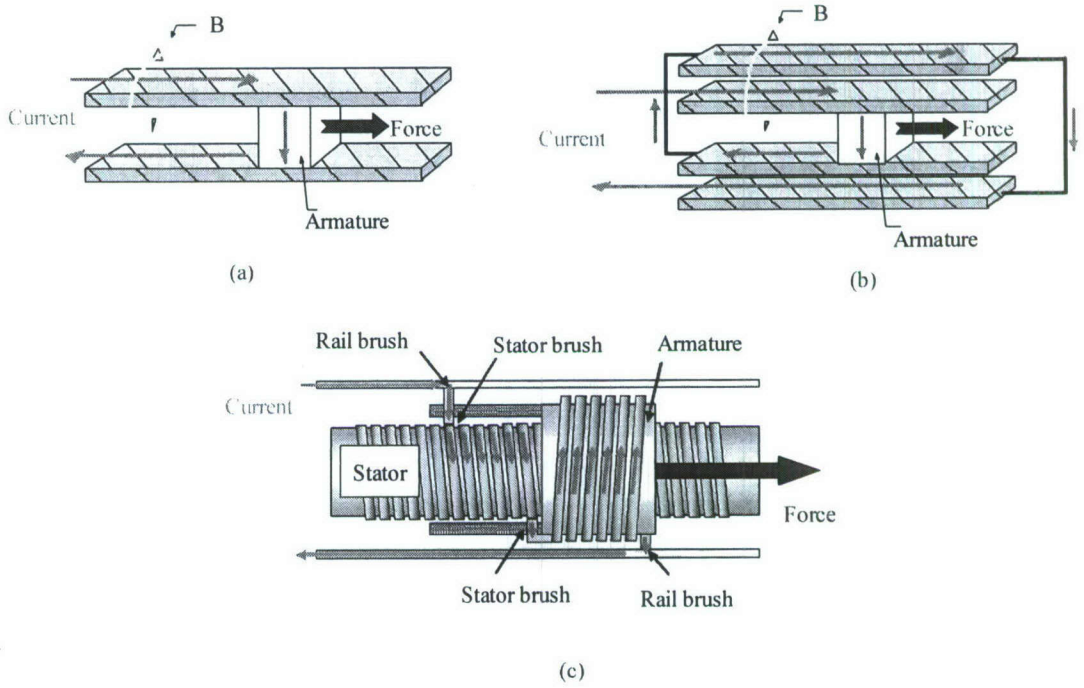

Fig. 7. The constant gradient EML geometry of the (a) conventional railgun, (b) augmented railgun, and (c) helical gun.

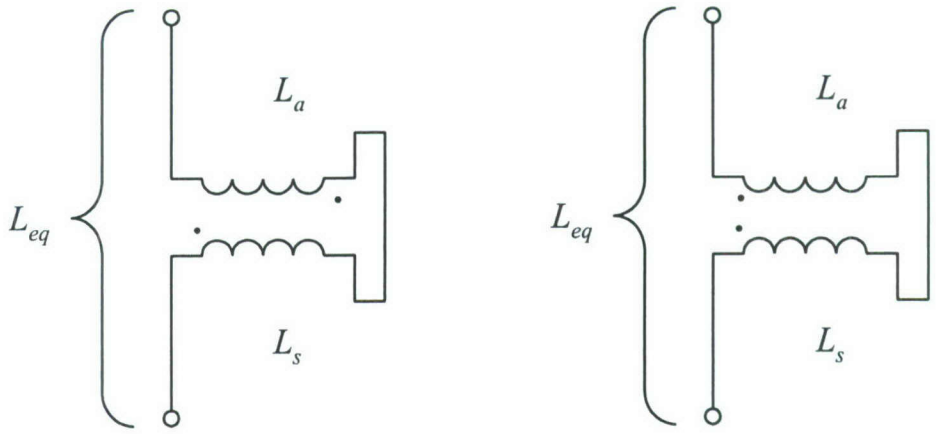

Fig. 8. The two electrical connections possible with helical gun geometry showing (a) additive magnetic fields and (b) subtractive magnetic fields.

$$\begin{aligned} F_{rg} &= \frac{d}{dx}\left(\frac{1}{2}LI^2\right) \\ &= \frac{1}{2}\frac{dL}{dx}I^2 \\ &= \frac{1}{2}L'I^2 \end{aligned} \tag{2}$$

where F_{rg} is the railgun force, L is the railgun inductance, L' is the railgun inductance gradient, and I is the railgun current. The helical gun geometry of Fig 7(c) primarily produces force between the armature-stator coil pair. The railgun force term of (2) is present in the helical gun, since the armature-stator coil pair form an equivalent armature, but is many times smaller than the helical gun force and can be ignored. To find the helical gun force, the total equivalent inductance of the armature-stator coil pair is needed and is given by coupled-coil relationship

$$\begin{aligned} L_{eq} &= \left(L_a \pm M\right) + \left(L_s \pm M\right) \\ &= L_a + L_s \pm 2M \end{aligned} \tag{3}$$

where L_a is the armature self-inductance, L_s is the stator self-inductance, and M is the mutual inductance between the armature and stator. In (3), the mutual inductance term will be positive for additive magnetic fields and negative for subtractive fields. Fig 8 illustrates the two helical gun circuit connections possible using standard coupled-coil notation. Differentiating (3) with respect to distance yields the helical gun inductance gradient

$$\begin{aligned}\frac{dL_{eq}}{dx} &= \frac{d}{dx}\left(L_a + L_s\right) \pm \frac{d}{dx}\left(2M\right) \\ &= \pm 2\frac{dM}{dx} \\ &= \pm 2M'\end{aligned} \tag{4}$$

where M' is the mutual inductance gradient. Positive M' indicates an attractive electromagnetic force while negative M' indicates a repulsive force. Since there is no change in L_a or L_s with respect to distance, these terms are not involved in force generation. Substituting (4) into (2) yields

$$\begin{aligned}F_{hg} &= \frac{1}{2}\frac{dL_{eq}}{dx}I^2 \\ &= M'I^2\end{aligned} \tag{5}$$

where F_{hg} is the helical gun force [4].

Kinetic Power

The three geometries of Fig 7 have current-carrying armatures moving through a magnetic field. When a conductor moves through a magnetic field, a voltage is induced at its terminals according to Faraday's law as

$$V_{ind} \triangleq -\frac{d\Psi}{dt} \tag{6}$$

where V_{ind} is the induced voltage and Ψ is the total flux linkage. Lenz's law gives the induced armature voltage polarity which can be safely ignored in this investigation. For the most general treatment, Faraday's law is expressed in terms of electric circuit parameters. Specific EML geometry information can be inserted at a later stage as needed. The induced armature voltage becomes

$$\begin{aligned}V_{ind} &= \frac{d\left(LI\right)}{dt} \\ &= L\frac{dI}{dt} + I\frac{dL}{dt} \\ &= V_e + V_b\end{aligned} \tag{7}$$

The first term of (7), V_e, is the usual inductor voltage produced when charging the inductor to a given energy state. The second term of (7), V_b, is the so-called back-voltage produced when performing mechanical work on the inductor, e.g., changing its shape or location in space.

The product of the back voltage and armature current is termed the kinetic power and represents the electrical power used to produce motion. The kinetic power for conventional and augmented railguns is found by multiplying the second term of (5) and the armature current given as

$$\begin{aligned} P_{krg} &= IV_b \\ &= I\left(I\frac{dL}{dt}\right) \\ &= I\left(I\frac{dL}{dx}\frac{dx}{dt}\right) \\ &= I^2L'v \end{aligned} \tag{8}$$

where P_{krg} is the railgun kinetic power and v is the armature velocity. Substituting the helical gun inductance gradient term of (4) into (8) yields the kinetic power expression for the helical gun

$$\begin{aligned} P_{khg} &= I\left(I\frac{dL_{eq}}{dx}\frac{dx}{dt}\right) \\ &= I^2L'_{eq}v \\ &= 2I^2M'v \end{aligned} \tag{9}$$

where P_{khg} is the helical gun kinetic power.

Efficiency

The constant gradient EML electric-kinetic conversion efficiency is defined as the ratio of the output energy and the total input energy given as

$$\eta \triangleq \frac{W_k}{W_k + W_r + W_i + W_c + W_f} \tag{10}$$

where η is the efficiency, W_k is the kinetic energy, W_r is the resistive energy losses, W_i is the inductive energy stored or lost to commutation (all other inductive energy storage is assumed zero), W_c is the contact energy losses, and W_f is the friction energy losses. High efficiency results if the kinetic energy is much greater than the sum of the resistive, inductive, contact, and frictional energy terms. Assuming efficient sliding contacts and negligible frictional losses, (10) can be further simplified to

$$\eta = \frac{W_k}{W_k + W_r + W_i} = \frac{1}{1 + \frac{W_r}{W_k} + \frac{W_i}{W_k}} \tag{11}$$

In applying (11) to the EMLs of Fig 7, consideration is given to the manner in which the launcher is operated since that determines its energy state and, subsequently, the substitutions for the various terms in (11). Two modes of operating the EML are considered. In the constant current (i.e., CC) mode, current is constant during the entire acceleration event interrupted only when the armature leaves the launcher. In the zero exit current (i.e., ZC) mode, current is increased to a given level but is zero as the armature exits the launcher. The current can decay to zero in a natural manner, as prescribed by the electrical circuit, or it can be forced to zero with an external circuit [5]. Mechanical methods physically interrupting current flow are not acceptable in the present context. The reason for this pertains to inductive energy storage in the launcher and will be detailed in the following section.

Constant Current Operation

The CC operation mode is applied to the conventional and augmented railgun. With constant I, the railgun force of (1) is integrated with respect to distance yielding the railgun armature kinetic energy

$$\begin{aligned} W_{krg} &= \int F_{rg}\, dx \\ &= \int \frac{1}{2}\frac{dL}{dx} I^2 dx \\ &= \frac{1}{2} L I^2 \\ &= W_{irg} \end{aligned} \tag{12}$$

where W_{krg} is the railgun kinetic energy and W_{irg} is the railgun inductive energy. Eq (12) shows that the railgun armature kinetic energy is equal to the inductively stored energy. Therefore, with $W_{krg} = W_{irg}$, (11) can be further reduced to

$$\eta_{rgcc} = \frac{1}{2 + \frac{W_{rrg}}{W_{krg}}} \tag{13}$$

where η_{rgcc} is the railgun efficiency in CC mode and W_{rrg} is the railgun resistive losses. Another expression for the railgun kinetic energy is needed for (13) and can be obtained by integrating the kinetic power in (8) with respect to time. In CC mode, the velocity

will increase linearly in time. Assuming the inductance gradient is constant, the result of this integration is given by

$$\begin{aligned} W_{krg} &= \int f_{rg} P_{krg} dt \\ &= f_{rg} \int \left(I^2 L' v \right) dt \\ &= f_{rg} \frac{1}{2} I^2 L' v_{\max} \tau \end{aligned} \tag{14}$$

where W_{krg} is the railgun kinetic energy, f_{rg} is the fraction of the kinetic power used to accelerate the railgun armature, $v_{\max}$ is the maximum armature velocity, and τ is the pulse length. The other fraction of the kinetic power is used to charge the railgun inductance. This statement is true because the power used to charge the inductor is included in the product of IV_b. The power is not in the product of IV_e since V_e is zero.

Rearranging the terms of (14) and substituting (2) yields

$$\begin{aligned} W_{krg} &= \left(\frac{1}{2} I^2 L' \right) f_{rg} v_{\max} \tau \\ &= F_{rg} f_{rg} v_{\max} \tau \end{aligned} \tag{15}$$

For consistency, the condition $f_{rg} = 1/2$ must be true, so that (15) will reduce to the expected result given by

$$\begin{aligned} W_{krg} &= F_{rg} \frac{1}{2} v_{\max} \tau \\ &= F_{rg} v_{avg} \tau \\ &= F_{rg} \Delta x \end{aligned} \tag{16}$$

where Δx is the length of the launcher. Since $f_{rg} = 1/2$, one-half of W_{krg} is converted to motion and one-half is stored inductively, as is already known from previous statements and (12).

A suitable expression for the resistive energy term in (11) is given by the definition

$$W_r \triangleq \int I^2 R dt \tag{17}$$

where R is the total system resistance. Assuming that R is also constant, then (17) becomes

$$W_{rcc} = I^2 R \tau \tag{18}$$

where W_{rcc} is the resistive energy losses. Constant system resistance is not true in practice because of joule heating and high frequency skin effects. An average system resistance can be used in these cases. Eqs (15) and (18) are substituted into (13) yielding railgun efficiency

$$\begin{aligned}\eta_{rgcc} &= \frac{1}{2+\dfrac{4I^2R\tau}{I^2L'v_{\max}\tau}} \\ &= \left(\frac{1}{2}\right)\frac{1}{1+\dfrac{2R}{L'v_{\max}}}\end{aligned} \tag{19}$$

The helical gun is the next EML geometry to be analyzed and suitable expressions are sought for the terms of (11). In CC mode, the helical gun force of (5) is integrated with respect to distance yielding the kinetic energy relationship of

$$\begin{aligned}W_{khg} &= \int F_{hg}dx \\ &= \int M'I^2dx \\ &= MI^2 \\ &= W_{ihg}\end{aligned} \tag{20}$$

where W_{khg} is the helical gun kinetic energy and W_{ihg} is the helical gun inductive energy lost during acceleration. Furthermore, assuming $L_{eq} \ll M$, there is no inductive energy stored since the helical gun uses only a short length of stator coil. The helical gun efficiency expression, therefore, has a form similar to the railgun efficiency of (13), namely

$$\eta_{hgcc} = \frac{1}{2+\dfrac{W_{rhg}}{W_{khg}}} \tag{21}$$

where η_{hgcc} is the helical gun efficiency in CC mode and W_{rhg} is the helical gun resistive losses. Proceeding as was done in (14), another helical gun kinetic energy expression can be found as

$$\begin{aligned} W_{khg} &= f_{hg}\int P_{khg}\,dt \\ &= f_{hg}\int\left(2M'I^2v\right)dt \\ &= \left(M'I^2\right)f_{hg}v_{\max}\tau \\ &= F_{hg}f_{hg}v_{\max}\tau \end{aligned} \tag{22}$$

where f_{hg} is the fraction of the kinetic power used to accelerate the helical gun armature. As before, the condition $f_{hg}=1/2$ must be true, so that (22) will reduce to $F_{hg}\Delta x$. One-half of W_{khg} is converted to motion and one-half is lost to commutation. Substituting (18) and (22) into (21) and rearranging terms yields the helical gun efficiency in CC mode as

$$\eta_{hgcc}=\left(\frac{1}{2}\right)\frac{1}{1+\dfrac{R}{M'v_{\max}}} \tag{23}$$

Zero Exit Current Operation

The ZC operation mode simplifies some of the previous analysis since there will be no inductive energy storage in the launcher at armature exit. If the current decays to zero naturally, as prescribed by the L/R time constant of the system, the inductive energy will be used toward acceleration. If the current is forced to zero with the aid of an energy recovery circuit [5], the inductively stored energy is removed from the system and the efficiency equation. In both cases, $W_i=0$ which reduces (11) to

$$\eta_{zc}=\frac{1}{1+\dfrac{W_r}{W_k}} \tag{24}$$

where η_{zc} is the efficiency in ZC mode. The launcher velocity is not linear since the current is not constant making direct integration in (14) and (22) impossible. In this mode of operation, we start with the familiar kinetic energy expression

$$W_k=\frac{1}{2}mv^2 \tag{25}$$

The momentum of the conventional and augmented railgun armature is given by

$$\begin{aligned} p_{rg} &= mv \\ &= \int F_{rg}\,dt \\ &= \frac{1}{2}L'\int I^2\,dt \end{aligned} \tag{26}$$

where m is the railgun armature mass and p_{rg} is its linear momentum. Substituting (26) into (25) yields the kinetic energy expression

$$\begin{aligned} W_{krg} &= \frac{1}{2}(mv)v \\ &= \frac{1}{4}L'v\int I^2 dt \end{aligned} \tag{27}$$

The resistive energy definition of (17) with constant system resistance becomes

$$W_{rzc} = R\int I^2 dt \tag{28}$$

where W_{rzc} is the resistive energy in ZC mode. Substituting (28) and (27) into (24) yields the conventional and augmented railgun efficiency

$$\begin{aligned} \eta_{rgzc} &= \frac{1}{1+\dfrac{R\int I^2 dt}{\dfrac{1}{4}L'v_{\max}\int I^2 dt}} \\ &= \frac{1}{1+\dfrac{4R}{L'v_{\max}}} \end{aligned} \tag{29}$$

where η_{rgzc} is the railgun efficiency in ZC mode. The substitution $v = v_{\max}$ is made since maximum efficiency is the only case of interest.

The efficiency for the helical gun EML operating in ZC mode is found by substituting the term $L' = L'_{eq} = 2M'$ in (29) to yield the final helical gun efficiency given as

$$\eta_{hgzc} = \frac{1}{1+\dfrac{2R}{M'v_{\max}}} \tag{30}$$

Comparing (2) and (5), the electromagnetic force is proportional to the square of the armature current. The force is also noted to be proportional to the inductance gradient of the EML geometry. Greater force can be produced by increasing the current a factor of 2, for example, than by increasing the inductance gradient a similar amount. Helical gun launchers have an additional factor of 2 in their force expression due to mutual inductance in comparison to railgun launchers.

The kinetic power expression given by (8) and (9) is the rate at which energy is delivered to the armature to produce acceleration and is the product of the armature current and the back-voltage. Like the mechanical force, the kinetic power is proportional to the square of the armature current. Unlike the electromagnetic force, however, the kinetic power is proportional to the armature velocity. The back voltage increases as the armature accelerates. As in the force expressions, helical gun launcher geometries have an additional factor of 2 in their kinetic power expression in comparison to railgun launchers.

The electromagnetic force and kinetic power *I*-squared dependency might lead one to conclude that high current EML operation is needed for large force production. While high current will certainly produce large kinetic power and force, it will simultaneously produce large resistive power loss. Eqs (19) and (29) clearly show that any increase in kinetic energy resulting from increased EML current is proportionally offset by increased resistive losses. High current EML operation should be avoided for high efficiency operation. The Experimental Results section will show that large electromagnetic forces can be generated with low current.

Examination of the railgun efficiency of (19) and (29) and the helical gun efficiency of (23) and (30) show that efficiency for these devices can be generalized to the expression

$$\begin{aligned}\eta &= \left(\frac{\mu}{4}\right)\frac{1}{1+\dfrac{\mu\lambda}{v_{\max}}} \\ &= \eta_{\max}\frac{1}{1+\dfrac{\mu\lambda}{v_{\max}}}\end{aligned} \tag{31}$$

where μ is a term reflecting the mode of operation ($\mu = \mu_{cc} = 2$ for CC mode and $\mu = \mu_{zc} = 4$ for ZC mode), λ is a term reflecting the launcher's geometry, and $\eta_{\max} = \mu/4$ is the maximum efficiency. In this investigation, μ is termed the *mode constant*, and λ is termed the *launcher constant*. The launcher constant is the ratio of the system resistance and the inductance gradient. For conventional and augmented railguns the launcher constant is given as

$$\lambda_{rg} = \frac{R}{L'} \tag{32}$$

whereas for helical guns the launcher constant is given as

$$\lambda_{hg} = \frac{R}{2M'} \tag{33}$$

Eq (31) shows that efficiency is clearly a function of the armature velocity. Although velocity-dependent EML efficiency will be experimentally verified in the following section, it should not be surprising since rotational DC motors are known to be inefficient in the start-up process [1]. The DC rotational motor has almost zero back-voltage (i.e., a short circuit) in the start-up phase with almost no electrical power being used to produce motion. As the motor gains speed, the back-voltage increases, more power is used for motion, and the motor approaches its steady-state efficiency. A similar scenario occurs for the EMLs in this investigation.

There are two limiting cases of efficiency in (31) with respect to velocity, specifically $v = 0$ and $v = \infty$. At low velocity, EMLs are inefficient while at high velocity, EMLs approach maximum efficiency. The EML back-voltage and kinetic energy are low at low velocity with little electrical power being used to produce motion. The resistive energy term dominates in (13) and (24) producing low efficiency. At high velocity, however, the back-voltage and kinetic power are high with a larger fraction of the electrical energy used to produce motion. The resistive energy term is negligible in comparison to the kinetic energy term and the efficiency is high.

Low velocity and *high velocity* are relative to the product of the mode constant and launcher constant. Normalizing (31) with respect to $\eta_{\max}$ yields the normalized EML efficiency of

$$\frac{\eta}{\eta_{\max}} = \frac{1}{1+\dfrac{\mu\lambda}{v_{\max}}} = \frac{1}{1+\dfrac{\sigma}{v_{\max}}} \tag{34}$$

where $\sigma = \mu\lambda$ is termed the *characteristic velocity*. If $v_{\max} \ll \sigma$, the velocity is considered low and the efficiency is low. If $v_{\max} \gg \sigma$, the velocity is considered high and the efficiency is high. When $v_{\max} = \sigma$, the launcher operates at 50% maximum theoretical efficiency.

Low σ geometries are synonymous with high efficiency. Fig 9 plots the normalized efficiency of (34) versus velocity for $\sigma = 1$, 10, 100, and 1000. As can be seen in that figure, low σ launchers approach maximum efficiency more quickly than high σ launchers. The characteristic velocity can, therefore, be used to characterize the EML. The launcher constant λ can also be used to characterize an EML if one assumes a fixed operating mode (i.e, CC or ZC) and armature velocity.

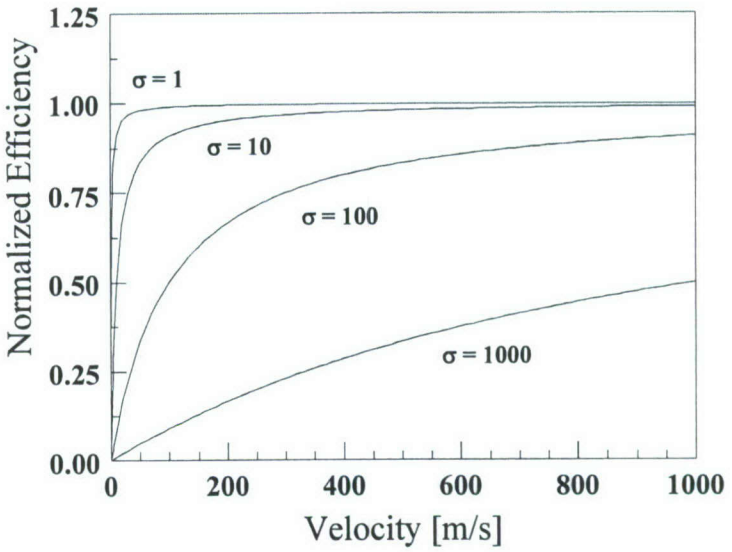

Fig. 9. Normalized efficiency versus velocity for various characteristic velocities.

The Fig 9 data also suggests that an *ideal launcher* is one that operates at 100% maximum efficiency, regardless of velocity. For example, a railgun or helical gun operating in CC mode at 50% efficiency would be considered an *ideal railgun* or an *ideal helical gun*. It would be unreasonable to define the ideal launcher as one that achieves 100% efficiency if the launcher is not operated in a mode that can attain 100% efficiency. Although the ideal launcher may be difficult to achieve in practice, the Fig 9 case with $\sigma = 1$ is very close to ideal and is approximately 90% normalized efficient for $v \geq 10$ m/s. In comparison, a launcher with $\sigma = 1000$ must operate at 10,000 m/s for 90% normalized efficiency. A low σ EML geometry approximates the ideal launcher.

The launcher constant is also a scaling factor reflecting the benefits derived when changes are made to a particular EML geometry. Specific EML geometry information can now be substituted in (31) or (34). Obviously, a low λ geometry is desired and is achieved by lowering the system resistance or increasing the inductance gradient.

Inductive energy use in constant gradient EMLs is determined by (12) and (20) that state regardless of operation mode, the EML will inductively store (or, consume) an energy equal to the kinetic energy of the projectile. If the EML is operated in the CC mode, then the stored energy is ultimately lost (either resistively as heat or acoustically as in arc blast when the projectile exits the launcher). If the EML is operated in ZC mode, then the stored energy can be used to accelerate the projectile or can be removed, or recovered, from the system.

A point to be made in this section regards the process by which different EML geometries are compared. From (34), the efficiency of a constant gradient EML is a function of both the armature velocity and the launcher's characteristic velocity. If the operation mode and armature velocity is fixed and the geometry has equal inductance

gradient and system resistance, the helical gun will be the most efficient geometry simply due to the additional factor of 2 in its launcher constant (c.f. (33)). However, EMLs should not be compared in this manner, since their physical size may be quite different indicating a difference in volumetric efficiency. To factor in both electric-kinetic conversion efficiency and volumetric efficiency, EML comparisons should be done with equal bore diameter, bore length, armature mass, and armature velocity. A comparison under these conditions is termed a *same-scale* comparison.

This section presents a *same-scale* comparative analysis of the experimental results with conventional railgun, augmented railgun [3], and helical gun EML geometries [5-8]. All the launchers are 40 mm bore diameter and 750 mm bore length. The launcher mass is on the order of 350 grams and all operate at approximately 150 m/s. Experimentally measured efficiency is given by

$$\eta = \frac{W_k}{W_u} = \frac{\frac{1}{2} m v_{\max}^{\ 2}}{W_0 - W_f} \tag{35}$$

where W_k is the kinetic energy of the projectile, W_u is the total electrical energy used, W_0 is the initial electrical energy stored in the PFN, and W_f is any electrical energy remaining in the PFN that is not used.

The first part of the analysis is an examination of efficiency versus velocity using the one-turn augmented railgun (ARG) data from Table IV. The ARG is powered by a single module pulse forming network (i.e, PFN) operating in ZC mode. Table IV lists the PFN charge voltage, peak armature current, armature velocity, and measured electric-kinetic efficiency for each of the ARG experiments. The measured efficiency and theoretical efficiency of (19) are plotted in Fig 10 versus velocity. The launcher constant used for plotting (19) is 300 [m/s] and is derived from static measurements of the inductance gradient ($L' = 1.2$ μH/m) and average system resistance ($R = 0.4$ mΩ) although both of these parameters are known to vary during the experiment. As can be seen in Fig 10, the velocity-dependent efficiency effect predicted by (19) is clearly evident. The ARG efficiency increases with velocity. The theoretical results are in good agreement with the experimental data at low velocity. There is 16.3% error between the predicted and measured results at the highest velocity. While this error is acceptable, it is attributed to increased system resistance from joule heating or decreased inductance gradient from high frequency skin effects. Both of these effects are present at high velocity because of the high current and because of the so-called velocity skin-effect [9].

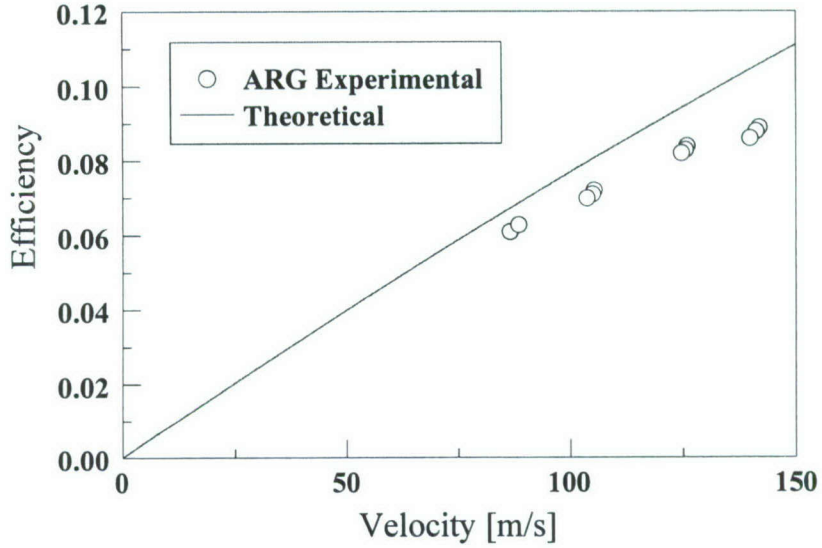

Fig. 10. Illustrating velocity-dependent efficiency for a one-turn augmented railgun.

The second part of the experimental data analysis is a comparative analysis of *same-scale* EMLs. Table II is a performance summary of a helical gun, a one-turn augmented railgun, and an ideal conventional railgun. Although there is some variation in the armature mass, the EMLs are considered same-scale with nominal 40 mm bore diameter, 750 mm bore length, 500 gram armature (i.e., projectile) mass, and 150 m/s velocity. Table II lists launcher specifications and experimentally measured data as well as static measurements of the inductance gradient and average system resistance.

TABLE IV
AUGMENTED RAILGUN (ARG) EXPERIMENTAL RESULTS

Experiment	V_{charge} [v]	I_{peak} [kA]	v_{max} [m/s]	η
1.1	1700	204	86.4	0.061
1.2	1700	204	86.4	0.061
1.3	1700	204	88.4	0.063
2.1	1900	226	105.2	0.072
2.2	1900	226	104.9	0.071
2.3	1900	226	103.6	0.070
3.1	2100	255	125.8	0.084
3.2	2100	255	125.5	0.083
3.3	2100	255	124.7	0.082
4.1	2300	270	141.8	0.089
4.2	2300	270	141.2	0.088
4.3	2300	270	139.7	0.086

The LCG-6 and LCG-7 data of Table V are helical gun experiments conducted with mechanically identical armatures. The difference between the armatures is the LCG-7 armature is liquid nitrogen cooled to reduce its resistance, whereas the LCG-6 armature is room-temperature with no cooling. The liquid nitrogen cooling reduced the armature resistance from 8.0 mΩ to 1.3 mΩ, a factor of almost 8 [8]. The armature resistance decrease reduces the system resistance approximately 40% (the stator resistance constitutes approximately 50% of the system resistance). The σ and λ values are directly proportional to the system resistance and are similarly reduced.

The CRG data of Table V are from a simulation of an ideal conventional railgun. The ideal CRG simulation is frictionless, lossless, and powered with an ideal constant-current source. While constructing a launcher to meet these specifications would be difficult, the absence of same-scale railgun investigations in the literature dictated the need for the simulation. The CRG inductance gradient and system resistance are conservative estimates based on [10] and the authors' experience with the ARG.

Pulsed power supplies for the LCG and ARG EMLs are capacitor based pulse forming networks (PFN's). The interested reader should consult [11] for PFN construction details. The V_{charge} data of Table V is the PFN charge voltage. The LCG-6 and LCG-7 experiments use an eight-module PFN and, therefore, had eight different charging voltages. The maximum and minimum module charge voltages are given in Table V. The ARG experiment used a single-module PFN, as stated previously.

The Table V data show the LCG-6 and LCG-7 EMLs to have an inductance gradient more than 2 orders of magnitude greater than the ARG and CRG launchers. In addition, the σ and λ values for LCG-6 and LCG-7 are more than an order of magnitude lower

TABLE V
ELECTROMAGNETIC LAUNCHER PERFORMANCE COMPARISON

Parameter	LCG-6	LCG-7	ARG	CRG
Bore diameter [mm]	40	40	40	40
Bore length [mm]	750	750	750	750
Projectile mass [g]	526	515	350	500
Inductance gradient [μH/m]	113	148	1.2	0.45
Operating mode	CC	CC	ZC	CC
R (min) [mΩ]	18.1	11.3	0.4	0.4
R (max) [mΩ]	21.9	12.1	2.0	0.4
R (avg) [mΩ]	20.0	11.7	0.4	0.4
λ [m/s] (Eq 32 or 33)	88	40	300	889
σ [m/s]	176	80	1200	1778
I_{peak} [kA]	12.4	11.5	270	183
V_{charge} [V]	300 to 550	250 to 550	2300	98
v_{max} [m/s]	137	164	141	150
Theoretical efficiency (Eq 19, 23, 29, 30) [%]	21.8	33.7	7.2	3.9
Measured efficiency [%]	18.2	32.0	8.8	3.9
Efficiency error [%]	16.6	5.1	16.3	0.0

LCG = long (i.e., helical) gun; ARG = augmented railgun; CRG = simulated ideal conventional railgun. See text for complete description of experiments.

than the ARG and CRG σ and λ values which means the LCG will be more efficient at fixed velocity, a fact verified in Table V. LCG-6 and LCG-7 are the most efficient launchers in Table V at 18.2% and 32%, respectively, and are the most efficient ever reported at this scale. The agreement between theoretical and experimental efficiency is good with a maximum error of 16.6% and a minimum error is 0% (exact agreement) with these errors attributed to changes in the σ and λ due to joule heating and/or skin effects. Thom and Norwood [12] also postulate that commutation effects could lower the effective inductance gradient of helical coil launchers.

Table V also lists the V-I operating characteristics of the various launchers. The LCG peak current is more than 20 times lower than the ARG peak current while accelerating a 40% larger mass. The maximum LCG PFN charge voltage is approximately 3 times lower than the ARG voltage. This, however, is misleading given the ARG operates in ZC mode. The ARG charge voltage would be comparable to the LCG voltage if it were operated in CC mode.

The CRG current is 16 times higher than the LCG current. The CRG operating voltage (operating voltage is used instead of PFN charge voltage since the CRG is driven with an ideal current source) is a factor of 5.6 lower than the maximum LCG voltage. It is only a factor of 2.6 lower than the minimum LCG voltage. Caution is used when interpreting this result since the CRG is powered with an ideal current source. A system resistance increase of 1 mΩ would increase the operating voltage 183 V from ohmic voltage drop (since $I = 183\,\text{kA}$). And considering that current is constant, Joule heating could easily increase the resistance by this amount. Table V data show the CRG is the most inefficient launcher considered in this investigation. This is not surprising given its σ of almost 1800 m/s. The large current needed for this velocity would almost certainly cause significant joule heating leading to larger σ and λ and, ultimately, lower efficiency. The combined evidence suggests that low σ and low λ launchers can not only be operated at significantly lower currents but at voltage levels that are slightly higher than (given an ideal power source) or comparable with (given a non-ideal power source) low gradient launchers.

The third part of this analysis consists of analyzing all the experimentally measured efficiency for the LCG launcher and comparing it to the theoretically predicted values. This data is listed in Table VI.

TABLE VI
SUMMARY OF LONG COIL GUN (LCG) EXPERIMENTAL RESULTS

Experiment	Bore [mm]	Mass [g]	M' [μH/m]	R / 2M ' [Ω•m/H]	I_{peak} [kA]	Velocity [m/s]	Efficiency [%]
LCG-1	20	125	40	128	12.4	45	2.2
LCG-2	20	158	19	454	13.8	21	0.8
LCG-3	20	166	45	333	11.3	56	3.3
LCG-4	40	428	163	254	13.5	82	8.7
LCG-5	40	519	151	225	14.8	97	13.2
LCG-6	40	526	113	88	12.4	137	18.2
LCG-7 *	40	515	148	40	11.5	164	32.0

Comparing the experimentally measured efficiency to the theoretical efficiency is done in Fig 11. As can be seen in that figure, there is good agreement between the theoretically predicted and experimentally measured efficiency.

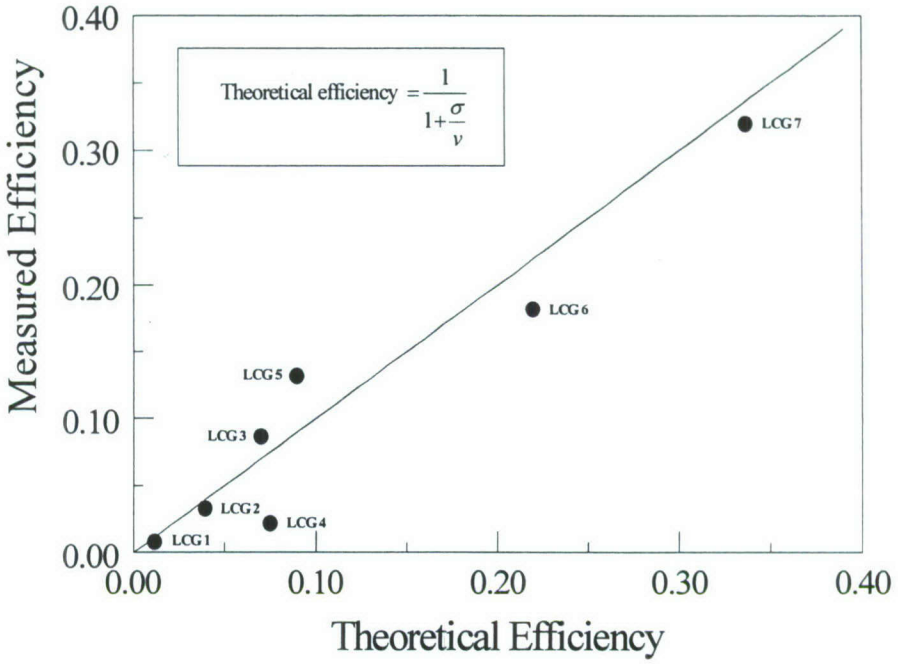

Fig 11. Comparing theoretical and experimentally measured efficiency.

General Theory of Electromagnetic Launcher Operating Point Selection

A general theory of EML operation is in order since the HCEL can be designed with any conceivable value of inductance gradient. Increasing the launcher's inductance gradient causes the EML to operate at a greater force for a given current. Significantly increasing the railgun's inductance gradient through changes in rail spacing or geometry is difficult, if not impossible. The use of augmentation turns to increase the inductance gradient is possible, but since the total system resistance (and operating voltage) will proportionally increase, the system efficiency will not increase (the efficiency of any constant-gradient EML is determined by the ratio of the total system resistance and the inductance gradient [3]). The helical EML geometry is an attractive alternative to the conventional and augmented railgun geometry since its inductance gradient and gradient/resistance ratio can be tailored to almost any value. Use of the helical EML geometry is the best method to reduce the EML current and, simultaneously, increase the EML efficiency.

This section details the design of a helical EML for the naval long-range bombardment application and the selection and control of the EML's V-I characteristics through selection of inductance gradient. The design of a sub-scale 3 MJ helical launcher to

demonstrate proof-of-principle is given along with the design of a full-scale 64 MJ constant gradient helical electromagnetic launcher. The full-scale helical EML requires only 1 MA peak current to launch a 20 kg projectile at 2500 m/s. This document also shows the versatility of the helical EML with the design of a variable-gradient, impedance matching helical EML for the full-scale application which reduces the peak launcher to only 700 kA. A high-efficiency helical EML geometry is also discussed and promises to reduce the launcher current below 700 kA level.

The table below lists the various launcher parameters for the sub-scale and full-scale helical EML designs in this document. The maximum kinetic-electric conversion efficiency in Table VIII is 50% which is determined by the launcher geometry. The conventional helical EML geometry shown in Fig 7 has a maximum efficiency of 50% and is the EML geometry used for designs in this document, unless otherwise stated. It is noted that this document describer only hollow-projectile helical EML designs. This should not be interpreted as a limitation of the helical EML since solid-projectile versions work in exactly the same manner and can be constructed as well.

TABLE VIII. SUB-SCALE AND FULL-SCALE HELICAL EML OPERATING PARAMETERS.

Parameter	Sub-Scale Design	Full-Scale Design
Launch mass	1 kg	20 kg
Barrel length	2 m	10 m
Barrel diameter	140 mm	140 mm
Muzzle velocity	2500 m/s	2500 m/s
Operating voltage	30 kV	30 kV
Electric-kinetic efficiency (max)	50%	50%

Sub-Scale (3 MJ) Launcher Design

The time required to accelerate a given mass to a given velocity with constant force is given by

$$\begin{aligned} \Delta t &= \frac{l}{v_{avg}} \\ &= \frac{l}{\frac{1}{2} v_{\max}} \\ &= \frac{2l}{v_{\max}} \end{aligned} \tag{36}$$

The force needed to launch a given mass is found from

$$
\begin{aligned}
F &= m\frac{\Delta v}{\Delta t} \\
&= m\frac{v_{\max}}{\Delta t}
\end{aligned}
\tag{37}
$$

Combining (36) and (37) yields

$$
F = \frac{mv_{\max}^2}{2l} \tag{38}
$$

The helical EML force can also be expressed by

$$
\begin{aligned}
F &= M'I^2 \\
I &= \sqrt{\frac{F}{M'}}
\end{aligned}
\tag{39}
$$

Neglecting resistive voltage drops, the helical EML operating voltage is given by

$$
\begin{aligned}
V_{back} &= 2M'vI \\
I &= \frac{V_{back}}{2M'v}
\end{aligned}
\tag{40}
$$

Equating (39) and (40) and solving for M' with a peak operating voltage of $V_{back} = 30\text{ kV}$, we have

$$
\begin{aligned}
\sqrt{\frac{F}{M'}} &= \frac{V_{back}}{2M'v_{\max}} \\
M' &= \frac{V_{back}^2}{4v_{\max}{}^2F} \\
&= \frac{lV_{back}^2}{2v_{\max}{}^4m} \\
&= \frac{2 \cdot \left(30\times10^3\right)^2}{2 \cdot 2500^4 \cdot 1} \\
&= 23.0\times10^{-6}\text{ H/m}
\end{aligned}
\tag{41}
$$

Using this value of M' in (39) yields a constant EML current of

$$
\begin{aligned}
I &= \sqrt{\frac{F}{M'}} \\
&= v_{\max}\sqrt{\frac{m}{2lM'}} \\
&= 2500\sqrt{\frac{1}{2 \cdot 2 \cdot 23\times 10^{-6}}} \\
&= 260\times 10^{3}\ \text{A}
\end{aligned}
\tag{42}
$$

The current in (42) is considered low and can be safely conducted by 1 contact. However, the current can be distributed over any number of armatures which has the following beneficial effects:

1. Reduces the current per contact.
2. Distributes the mechanical forces.
3. Reduces resistance increase from joule heating.

Assuming 3 armatures arranged in a series/parallel connection, the current per contact will be reduced to 87×10^{3} A. The projectile muzzle energy is found as

$$
\begin{aligned}
W &= \frac{1}{2}mv^{2} \\
&= \frac{1}{2} \cdot 1 \cdot 2500^{2} \\
&= 3.1\times 10^{6}\ \text{J}
\end{aligned}
\tag{43}
$$

The maximum total system resistance to achieve this level of performance can be found from the helical launcher efficiency relationship given as

$$
\eta = \eta_{\max}\frac{1}{1+\dfrac{R_{sys}}{v_{\max}M'}} \tag{44}
$$

where $\eta_{\max} = 50\%$ for the conventional helical EML geometry (see Fig 7). It's practically impossible for the helical launcher to operate at 50% efficiency since that would require an extremely low R_{sys}. Instead, we opt for an efficiency of 45% so that (44) becomes

$$0.45 = 0.50 \frac{1}{1 + \dfrac{R_{sys}}{v_{\max} M'}}$$

$$R_{sys} = v_{\max} M' \left[\left(\frac{0.50}{0.45} \right) - 1 \right] \tag{45}$$

$$= 2500 \cdot 23 \times 10^{-6} \left[\left(\frac{0.50}{0.45} \right) - 1 \right]$$

$$= 6.4 \times 10^{-3} \Omega$$

The voltage increase caused by system resistance is given by IR_{sys} and amounts to $6.4 \times 10^{-3} \cdot 260 \times 10^{3} = 1.7 \times 10^{3}$, which is insignificant compared to the back-voltage. The estimates above do not include effects produced by joule heating of the conductor. Therefore, the estimates need to be verified with numerical models developed by the author. The author's computer models accurately calculate the helical coil resistance, inductance and inductance gradient using the actual physical dimensions and include resistance changes from joule heating effects from 1 K to 1000 K. The simulation conditions and results are listed in Table IX.

TABLE IX. SUB-SCALE HELICAL EML SIMULATION CONDITIONS AND RESULTS.

Parameter	Value
Launcher	
Type	Hollow projectile
Number of armature-stator coil pairs	1
Length	2 m
Inductance gradient	22.5 μH/m
Voltage (peak)	31.8 kV
Current (ideal source, constant)	270 kA
Acceleration time	1.58 ms
Efficiency	45.4 %
Projectile	
Mass	1 kg
Velocity	2514 m/s
Acceleration	168 kGee
Armature coil (inside projectile)	
Material	Cu
AWG	1
Radius	78.1 mm (3.075 in)
Axial length	20.1 mm (0.791 in)
Resistance (min/max)	0.36 / 1.14 mΩ
Number of turns	1.6
Mass	0.31 kg
T (initial)	294 K (21 °C)
T (final)	976 K (703 °C)
Radial stress	18.1 GPa
Stator coil (inside barrel)	
Material	Cu
AWG	3
Radius	69.9 mm (2.752 in)
Axial length	47.1 mm (1.854 in)
Resistance	2.0 mΩ
Number of turns	6.4
Mass	---
Radial stress	36.9 GPa

The simulation shows the parasitic mass ratio (armature mass to projectile mass) to be 31%. The armature temperature increases from 294 K to 976 K. The melting point of pure copper is 1353 K (1080 °C). The large armature radial force of 18.1 GPA indicates that e-glass or carbon-fiber reinforcement is needed to contain the armature.

Full-Scale (64 MJ) Launcher Design

Scaling the helical EML to larger mass and velocity is done using (41) and (42). The full-scale (64 MJ) long-range bombardment application uses a 20 kg mass at 2500 m/s and a 10-meter launcher length. With an operating voltage of 30 kV, the inductance gradient is given by (41) as

$$\begin{aligned} M' &= \frac{lV_{back}^2}{2v_{\max}{}^4 m} \\ &= \frac{10 \cdot \left(30\times10^3\right)^2}{2 \cdot 2500^4 \cdot 20} \\ &= 5.8\times10^{-6}\ \text{H/m} \end{aligned} \tag{46}$$

and the operating current is given by (42) as

$$\begin{aligned} I &= v_{\max}\sqrt{\frac{m}{2lM'}} \\ &= 2500\sqrt{\frac{20}{2 \cdot 10 \cdot 5.8\times10^{-6}}} \\ &= 1.0\times10^6\ \text{A} \end{aligned} \tag{47}$$

As in the sub-scale demonstrator, the total launcher current can be distributed amongst any number of series/parallel connected armatures. The helical EML design has the potential to reduce the rail erosion problem of conventional railguns. In addition, while the railgun force is present in the helical EML, it is 25 times smaller than the helical gun force and can be ignored. Table X summarizes the simulation results of the full-scale helical EML.

The maximum total system resistance to achieve this level of performance can be found from the helical launcher efficiency relationship of (44). With $\eta = 45\%$, the total system resistance is found as

$$\begin{aligned} R_{sys} &= v_{\max}M'\left[\left(\frac{0.50}{0.45}\right)-1\right] \\ &= 2500 \cdot 5.8\times10^{-6}\left[\left(\frac{0.50}{0.45}\right)-1\right] \\ &= 1.6\times10^{-3}\Omega \end{aligned} \tag{48}$$

The voltage increase caused by system resistance is given by IR_{sys} and amounts to $1.6\times10^{-3} \cdot 1\times10^6 = 1.6\times10^3$, which, again, is insignificant compared to the back-voltage. The acceleration for the full-scale launcher is given as

$$a = F/m = MI^2/m = \left(5.8\times10^{-6}\right)\left(1.0\times10^{6}\right)^2/20 = 30 \text{ kGee} \quad (49)$$

TABLE X. THEORETICAL SUB-SCALE AND FULL-SCALE HELICAL EML OPERATING PARAMETERS.

Design	V_{max}	$I_{constant}$
Sub-scale (3 MJ)	30 kV	260 kA
Full-scale (64 MJ)	30 kV	1 MA

Liquid Nitrogen Cooled Armature

This section describes the advantages associated with cooling the armature of the HCEL to decrease the total system resistance and improve the EML's electric-to-kinetic energy conversion efficiency. Experimentally, we have demonstrated 165 m/s launch with the 40 mm HCEL. The typical projectile mass for these experiments was approximately 520 grams. Measurements show an electrical-to-kinetic conversion efficiency of 32 % which is the highest efficiency ever reported for this launcher scale. The high efficiency was achieved because the armature windings were cooled with liquid nitrogen. With cooling, the armature resistance was decreased by a factor of eight thereby eliminating a large electrical loss. For comparison purposes, an identical armature operating at room temperature can achieve 18 % efficiency. Thus, the liquid nitrogen cooling almost doubled the efficiency. Fig 12 shows a close-up of the 40 mm HCEL liquid nitrogen cooled and room-temperature armatures.

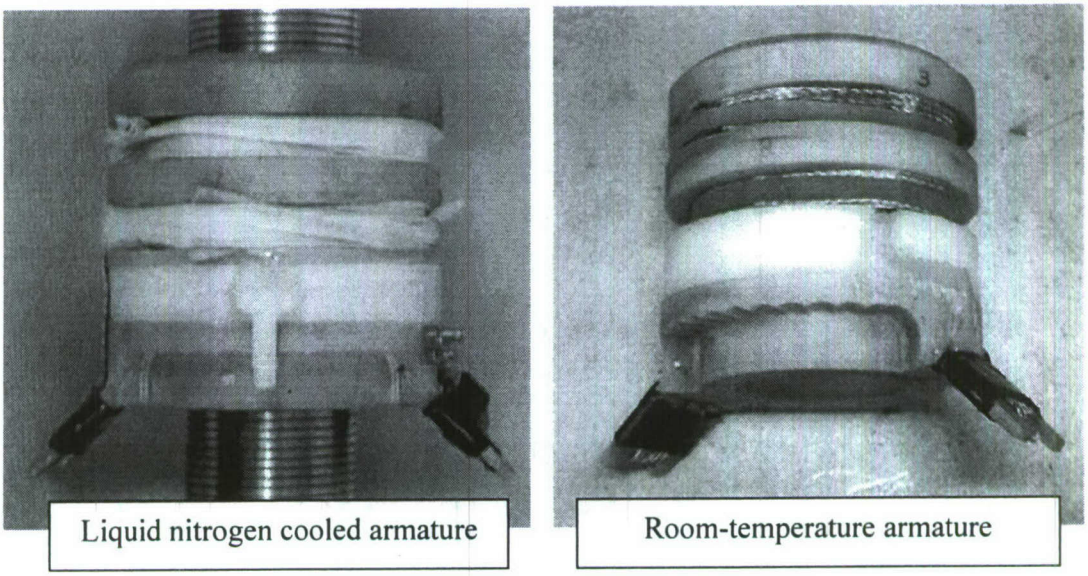

Fig 12. Liquid nitrogen cooled and room temperature HCEL armatures.

Hall-Effect Switch Model Development

The magnetically-controlled Hall-effect switch (HES) has obvious applications in EML technology since the EML's magnetic field is quite large (i.e., 10 to 100 Tesla). Suitable HESs could have enormous impact on EML performance, especially the performance of helical and coil launchers. The HES would not only reduce parasitic mass and improve the reliability by eliminating the need for stator brushes, it would also increase the EML efficiency by increasing the inductance gradient to system resistance ratio an order of magnitude. However, HES technology is only in its infancy. Computer modeling tools had to be developed to understand the potential of this technology.

The effect of the magnetic field in the HES is simulated by the two voltage controlled current sources F_{xy} and F_{yx} which apply the gain represented by the σ_{xy} and σ_{yx} terms to the voltage sensed across the element normal to the direction of current flow in the finite-element model implemented in PSpice shown in **Fig**3.

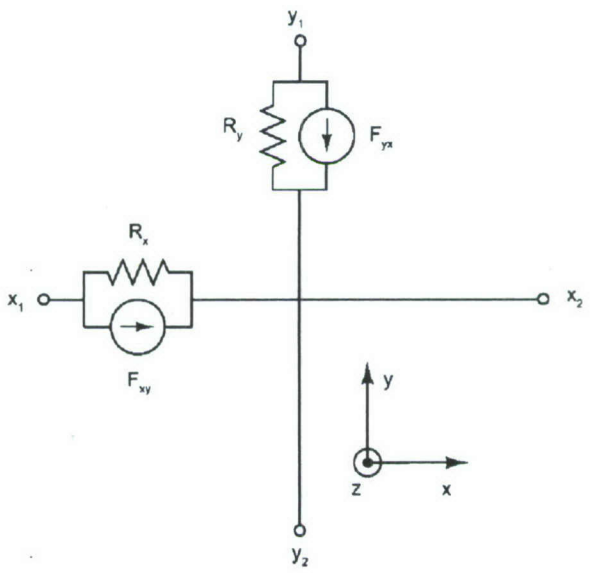

Fig 13. Semiconductor unit cell of the HES equivalent circuit model showing the conventional elements: a resistor and a current source for the x and y dimensions.

For example,

$$I(F_{xy}) = \left(\frac{\sigma_{xy}}{\Delta y}\right)\left[V(y_1) - V(y_2)\right]$$

A complete HES is shown in Fig 14.

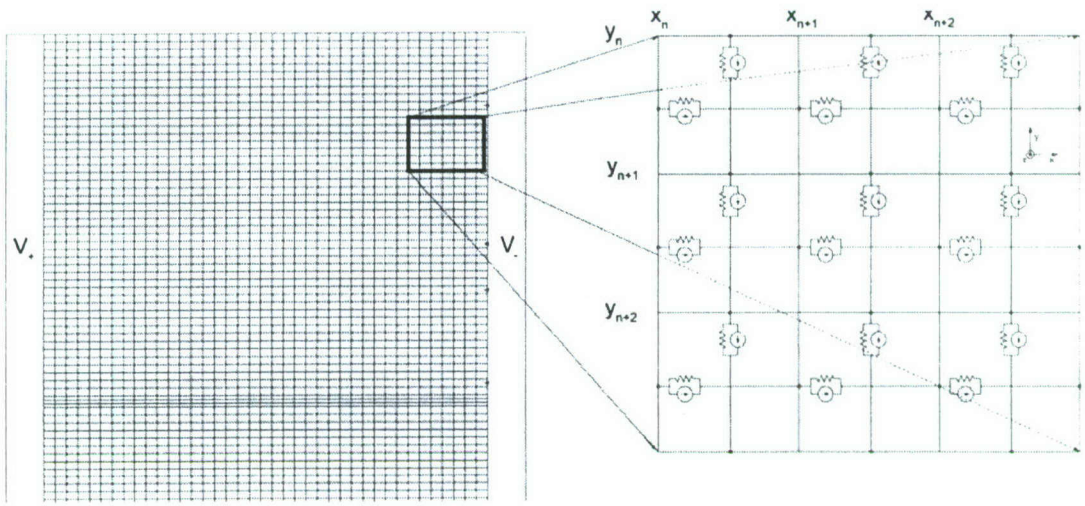

Fig 14. Electrical network used to model the electrical properties of a simple HES with inset of constituent unit cells.

The magnetoresistance estimated by the computer model is shown in Fig 15 and in good agreement with that obtained experimentally.

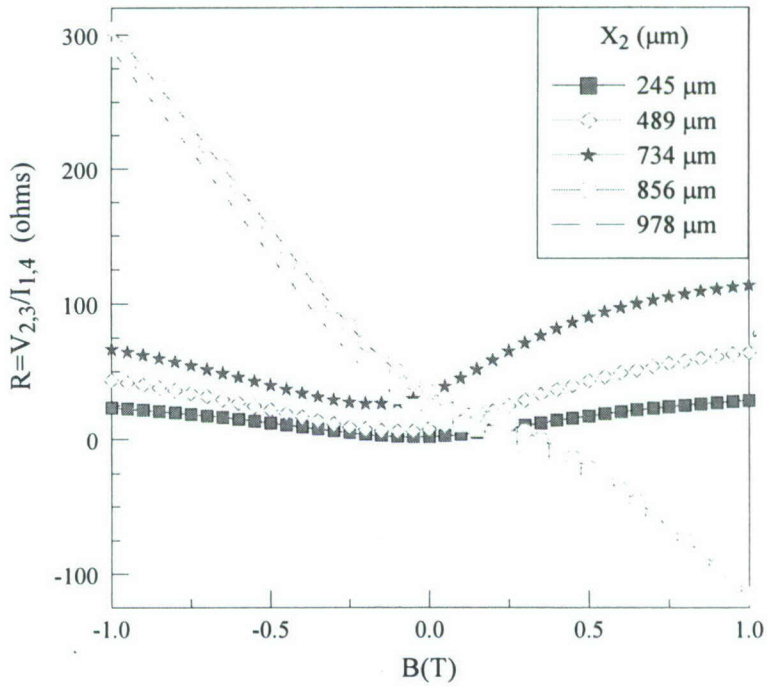

Fig 15. Resistance derived from different placement of voltage port 3 referenced to port 2 when placed at the midpoint (x1=0). The current injection ports (1 and 4) are held at constant position (x3=x4=795μm).

Summary and Conclusions

The research presented here develops a general theoretical efficiency and scaling relationship for constant gradient EMLs from basic principles expressing those relationships in terms of electrical circuit parameters. EML efficiency is shown to be a function of the armature velocity and the launcher's characteristic velocity. The characteristic velocity completely characterizes the launcher since it is the product of the mode constant and the launcher constant. The EML must operate at its characteristic velocity to achieve 50% maximum theoretical efficiency.

The launcher constant is derived here and is the ratio of the system resistance and inductance gradient. The launcher constant is a scaling factor and a figure of merit which also characterizes the EML. As a scaling factor, it can be used to predict performance gains derived through changes in the EML geometry (i.e., system resistance and inductance gradient). As a figure of merit and with fixed operating mode and armature velocity, the launcher constant is useful when comparing launchers of different geometry.

The two modes of EML operation theoretically considered in this investigation are; constant current mode and zero exit current mode. The mode constant reflects the operating mode and determines the maximum EML efficiency. The maximum EML efficiency in constant current mode is 50% while the maximum EML efficiency in zero exit current mode is 100%. Inductive energy is stored in the launcher in constant current mode. Zero exit current mode allows any inductively stored energy to be used toward accelerating the armature or to be removed from the system.

The concept of an ideal launcher is developed in this investigation. The ideal launcher operates at 100% of its maximum theoretical efficiency at all velocities. A low or low geometry approximates the ideal launcher. This investigation also shows that EML comparisons should be done on a same-scale basis, meaning equal bore diameter, bore length, armature mass, and velocity. Same-scale comparisons account for both electric-kinetic conversion efficiency and volumetric efficiency.

A comparative analysis of a same-scale conventional railgun, augmented railgun, and helical gun is presented. The comparative analysis verifies that efficiency is a function of armature velocity and shows that low or low geometries, such as the helical gun, are many times more efficient than conventional and augmented railguns. Furthermore, the comparative analysis shows that low σ or low λ EMLs can operate at an order of magnitude lower current and with voltage comparable to or slightly higher than conventional and augmented railguns. High efficiency EML geometries are desirable from a systems point of view since they reduce the primary power requirements, the size of the PFN, the switching requirements and, although not investigated here, the cooling requirements and lifetime of the launcher.

In regards to experimentally measured efficiency, the 40 mm HCEL investigated in this research was many times more efficient than same-scale conventional railguns or augmented railguns operating at 150 m/s. The liquid nitrogen cooled HCEL was

approximately 2 times more efficient than the room-temperature HCEL, approximately 4 times more efficient than a one-turn augmented railgun, and approximately 8 times more efficient than a conventional railgun. Super- or cryo-cooling the EML conductors is an effective method to improve the performance and efficiency of the HCEL provided, of course, that the cooling methods can be implemented in a practical manner. The peak current requirements for the HVEL is 16 times lower than the conventional railgun and more than 20 times lower than a one-turn augmented railgun. The HCEL operating voltage is approximately 3 times lower than the one-turn augmented railgun but a factor of 5.6 higher than a conventional railgun.

A theoretical basis to control the EML's V-I characteristics by judicious choice of inductance gradient is developed in this investigation. The theoretical basis is used to design a helical EML for the U.S. Navy's long-range bombardment application. While the design focuses on the electrical aspect of the launcher and uses a 50% maximum efficiency geometry, the HCEL is shown to operate at 1 MA peak compared to the 6 MA required by the conventional railgun geometry. The HCEL operates at a significantly lower current because its V-I operation point is controlled by careful selection of inductance gradient. It is noted that the HCEL operates at 30 kV compared to the 15 kV operation of the conventional railgun. Needless to say, the significantly lower operating current will result in lower brush and rail erosion. Acceleration forces can also be distributed within the HCEL armature by using multiple armature-stator coil pairs which reduces the projectile's parasitic mass ratio and provides magnetic levitation to the projectile. The mechanical aspects of the HCEL design should be investigated in the future.

The hall-effect switch model predicted the experimentally-measured magnetoresistance to a good degree of accuracy. The switch model enables the engineer to predict device physics and include that behavior in larger circuits and systems. The large magnetic field present in most electromagnetic launchers makes Hall-effect devices a natural choice. Presently, semi-conductor mobility and carrier concentrations limit the device to low magnetoresistance.

References

[1] Naval Research Laboratory, N00173-05-C-2048.

[2] D. Brown and E.P. Hamilton, *Electromechanical Energy Conversion*, MacMillan Publishing, NY, 1984.

[3] T.G. Engel, J. M. Neri, W.C. Nunnally, "Efficiency and scaling of constant inductance gradient DC electromagnetic launchers," *IEEE Transactions on Magnetics*, vol. 42, no. 8, pp 2043 – 2051, 2006.

[4] T.G. Engel, et al., "Prediction and verification of electromagnetic forces in helical coil launchers," *IEEE Transactions on Magnetics*, vol. 39, no. 1, pp. 112-115, 2003.

[5] E.M. Honig, "Switching considerations and new transfer circuits for electromagnetic launch systems," *IEEE Transactions on Magnetics*, vol. 20, no. 2, pp. 312-315, 1984.

[6] T.G. Engel, et al., "Research progress in the development of a high-efficiency, medium-caliber helical coil electromagnetic launcher," *Proc. 12th Symposium on Electomagnetic Launch Technology*, pp. 49-52, 2004.

[7] T.G. Engel, et al., "High-efficiency, medium-caliber helical coil electromagnetic launcher," *IEEE Transactions on Magnetics*, vol. 41, no. 11, 2005.

[8] T.G. Engel, et al., "Medium-bore helical-coil electromagnetic launcher with liquid nitrogen cooled armature," to appear *Proc. 15th IEEE International Pulsed Power Conference*, June 2005.

[9] R.A. Marshall and W. Ying, *Railguns: Their science and technology*, China Machine Press, Beijing, 2004.

[10] I.R. McNab, et al., "Development of a naval railgun," *IEEE Transactions on Magnetics*, vol. 41, no. 1, pp. 206-210, 2005.

[11] T.G. Engel and W. Clay Nunnally, "Sequentially-fired capacitive pulse forming network for non-linear loads," *IEEE Transactions on Plasma Science*, vol. 33, no. 6, 2005.

[12] K. Thom and J. Norwood, Jr., "Theory of an electromagnetic mass accelerator for achieving hypervelocities," *NASA Technical Note*, D-886, 1961.